17th World Conference on Earthquake Engineering, 17WCEE
Sendai, Japan - September 13th to 18th 2020

Estimation of Earthquake Ground Motions by Mega-quake along Nankai Trough for Structural Design in Tokai Region, Japan

M. Mori[(1)], N. Fukuwa[(2)], T. Nishizawa[(3)], K. Umemura[(4)], J. Miyakoshi[(5)], A. Oana[(6)], K. Dan[(7)], H.Takahashi[(8)], S. Ito[(9)]

[(1)] *Designated Professor, Nagoya Univ., D.Eng., m.mori@nagoya-u.jp*
[(2)] *Professor, Nagoya Univ., D.Eng., fukuwa@nagoya-u.jp*
[(3)] *Associate, Nikken Sekkei, D.Eng., nishizawa@nikken.jp*
[(4)] *Senior Manager, Takenaka Corp., M.Eng., umemura.kenji@takenaka.co.jp*
[(5)] *General Manager, Ohsaki Research Institute, Inc., D.Eng., miya@ohsaki.co.jp*
[(6)] *Researcher, Ohsaki Research Institute, Inc., D.Eng., a.oana@ohsaki.co.jp*
[(7)] *Research Fellow, Ohsaki Research Institute, Inc., D.Eng., dan@ohsaki.co.jp*
[(8)] *Associate Professor, Meijo Univ., D.Eng., hirohito@meijo-u.ac.jp*
[(9)] *Aichi Building Housing Center, ito@abhc-mail.jp*

Abstract

We reported the background of the project for the design earthquake ground motion estimation in the Tokai area, Japan, for the Nankai Trough earthquake prepared for the Aichi Prefecture Design Input Earthquake Ground Motion Research Council. We showed the assumed source region, fault models, and evaluation results. Eleven sites were selected in the Tokai area, and the empirical Green's function method was applied to the prediction of the strong motions. As stress drops on the asperities of the fault model, three cases (Cases 1,2,3) were provided due to the uncertainty of the short-period level. Case 1 is called as the fundamental case in this paper.

Calculated ground motions were compared with the seismic intensity of past large earthquakes along the Nankai Trough and some results of ground motion evaluations by other organizations. Then, the ground motions on the building foundation of Case 1 were calculated at one of the sites by using the nonlinear seismic response analyses of surface soil. Furthermore, with the ground motions above mentioned, we performed nonlinear response analyses of some virtual buildings such as high-rise buildings and base-isolated buildings. We showed the results of the parametric study, in which we considered different number of floors of buildings, earthquake resistance strengths, damping factors, natural periods, and base isolation devices. We found that amplitudes of some estimated input ground motions were large but these were levels that we can perform the seismic design by appropriate measures for both high-rise buildings and base isolated buildings.

Keywords: Empirical Green's function method, high-rise building, Base-Isolated building, Response characteristics

1. Introduction

The Aichi Prefecture Design Input Earthquake Ground Motion Research Council (hereinafter the "Council") [1] launched a study of design input ground motions in 2010, incorporating the latest knowledge about earthquakes that have occurred along the Nankai Trough. This aimed at revising ground motions by Nankai Trough earthquakes for the seismic design of buildings in the Tokai region. Initially, the Tokai/Tonankai earthquake was considered as the basis of the study, but as a result of the 2011 off the Pacific coast of Tohoku earthquake, a review of the expected source area and ground motion estimates in the Nankai Trough earthquake were conducted by the Cabinet Office [2,3], and so the source area was changed from the Tokai/Tonankai area (same as that of the 1854 Ansei-Tokai earthquake) to the Nankai Trough mega-quake area reported by the Cabinet Office [2,3].

In addition, concerning long-period ground motions, which are considered as a subject for further study, the Cabinet Office [4] published a report on long-period ground motions from the mega-quake along the Nankai Trough in December, 2015. Based on the results of the study by the Cabinet Office, the Ministry of Land, Infrastructure, Transport and Tourism (MLIT) [5] published countermeasures against long-period

ground motions for high-rise buildings based on the Building Standards Act (Act No. 201 of 1950) as a notification on June 24, 2016, after collecting public comments in December, 2015. The Cabinet Office assumed an expected source area that includes strong motion generation areas of past Nankai Trough earthquakes such as the 1707 Hoei earthquake, the 1854 Ansei-Tokai earthquake, the 1944 Tonankai earthquake, and the 1946 Nankai earthquake. On the other hand, MLIT considered the source area of the 1707 Hoei earthquake as the expected source area.

This paper describes the estimated ground motions and the building response evaluations, comparing the ground motions by the Cabinet Office and MLIT. Specifically, the 1707 Hoei earthquake was used as the scenario earthquake, and a fault model assuming this earthquake was established to evaluate the input ground motion. At this time, three cases (Cases 1 to 3 as shown in Section 3.2) with three different short-period levels were assumed because, even in the same source area, the possibility of ground motions with different seismic intensities cannot be excluded.

Regarding the ground motion evaluation method, many ground motion records were observed by the strong ground motion observation network [6], so we decided to adopt the empirical Green's function method by using these records. The generated ground motions were verified in comparison with seismic intensity distributions of past earthquakes. In addition, to confirm the behavior of buildings with respect to the generated ground motions, seismic response analyses for high-rise buildings and seismic-isolated buildings were performed.

2. Ground motion evaluation sites

Fig.1 shows ground motion evaluation sites. Eleven sites were selected in Tokai region from Ise Plain to Hamamatsu City so that seismic observation records and ground survey data could be used and that the deep subsurface dominant period of each site may distribute as diversely as possible. The primary dominant periods of the deep subsurface from the seismic basement to the engineering bedrock are superimposed on this figure. From this figure, the selected ground motion evaluation sites have a wide variety of different primary dominant periods.

3. Establishment of scenario earthquake and fault models

3.1 Scenario earthquake and expected source area

The scenario earthquake was assumed that the largest earthquake in the past at the source area which would most likely occur along the Nankai Trough in the future. Referring to the fault model of the 1707 Hoei earthquake given by the Cabinet Office [4], the source area of the scenario earthquake was extracted from the source area of the Nankai Trough mega-quake hypothesized by the Cabinet Office [7] including both regions of which focal depths were shallower than 30 km and the strong motion generation area at the west end of the source area assigned by the Cabinet Office [4]. Hereinafter, this scenario earthquake is called “the Hoei-type earthquake”.

3.2 Establishment of fault models

The fault parameters of asperity models for the Hoei-type earthquake were set based on the fault parameter setting method for the strong ground motion prediction of plate-boundary earthquakes proposed by Dan *et al.* [8] under condition that the fault area was given. Here, the short-period levels were calculated with reference to the short-period level of the 2011 off the Pacific coast of Tohoku earthquake and the strong ground-motion prediction recipe (“Recipe”) published by the Headquarters for Earthquake Research Promotion [9]. The short-period level of the 2011 off the Pacific coast of Tohoku earthquake (e.g., Sato [11], Kawabe and Kamae [12], and Kurahashi and Irikura [13]) is considered to be about 1 to 2 times larger than that calculated from the empirical relationship between the seismic moment and the short-period level for crustal earthquakes by Dan *et al.* [10]. In addition, the strong ground-motion prediction recipe (“Recipe”) [9] noted that if the short-period level of the latest earthquake activity in the expected source area has not been estimated, the short-period level is considered to be set according to the empirical relationship [10] between

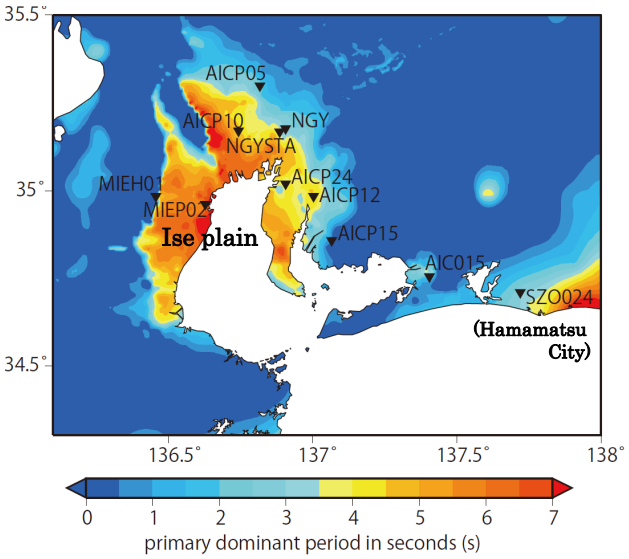

Fig. 1 – Primary dominant periods of deep subsurface and ground motion evaluation sites

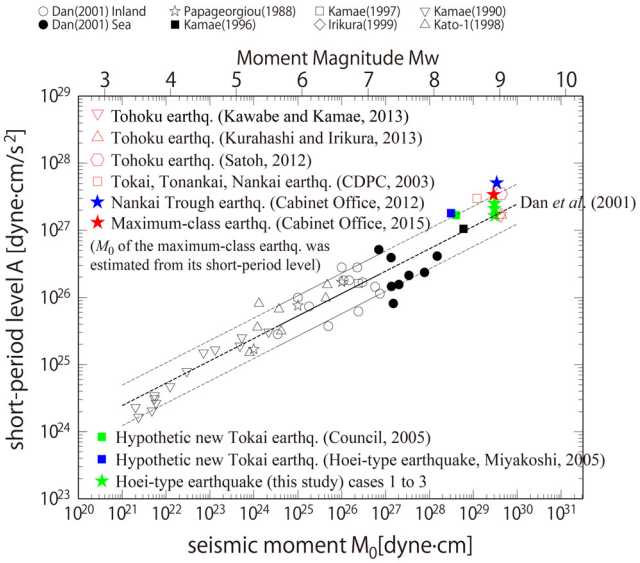

Fig. 2 – Relationship between seismic moment and short-period level

the seismic moment and the short-period level for crustal earthquakes.

Based on the above, in this study, we assumed three cases of 1, 1.25, and 1.5 times the average short-period level of the empirical relationship by Dan *et al.* [10] as Case 1 (fundamental case), Case 2, and Case 3, respectively. Fig.2 shows the relationship between the short-period level and the seismic moment. As shown in this figure, the short-period levels of the Tokai/Tonankai/Nankai earthquakes estimated by the Central Disaster Management Council [14], the Nankai Trough mega-quake estimated by the Cabinet Office [7], and the maximum class of the Nankai Trough earthquake calculated by the Cabinet Office [7] are larger than that of Case 3 in this study. In addition, the short-period level of the new Tokai earthquake assumed by Miyakoshi *et al.* [15] and the Council [16] is intermediate between those of Case 1 and Case 2 in this study. Table 1 shows the Hoei-type earthquake's fault parameters.

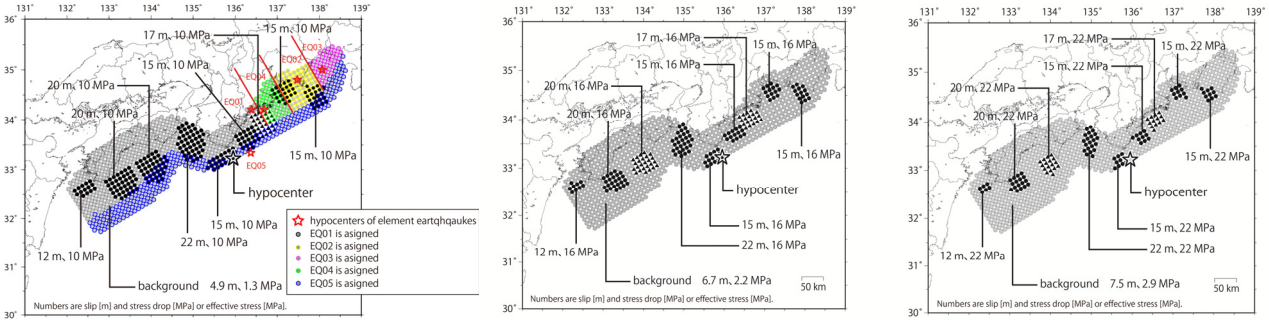

(a) Case 1 (b) Case 2 (c) Case 3

Fig. 3 – Fault models of the Hoei-type earthquake

Table 1 –Fault parameters of the Hoei-type earthquake

fault area	seismic moment	averaged stress drop	short-period level	asperity area	asperity stress drop	averaged slip on asperities	slip on background	effective stress on background
S	M_0	$\Delta\sigma$	A	S_{asp}	$\Delta\sigma_{asp}$	D_{asp}	D_{back}	σ_{back}
[km^2]	[Nm]	[MPa]	[dyne·cm/s^2]	[km^2]	[MPa]	[m]	[m]	[MPa]
case 1 same short-period level as empirical relationship for crustal earthquakes								
83772	3.05E+22	3.07	1.66E+20	25753	10.0	17.8	4.9	1.3
case 2: 1.25-time short-period level by empirical relationship for crustal earthquakes								
83772	3.05E+22	3.07	2.07E+20	16482	15.6	17.8	6.7	2.2
case 3: 1.5-time short-period level by empirical relationship for crustal earthquakes								
83772	3.05E+22	3.07	2.48E+20	11446	22.4	17.8	7.5	2.9

We assumed μ=4.10×10^{10} N/m^2 and β=3.82 km/s.

The asperity locations of the fault models were taken from the report of Cabinet Office [4] and the rupture starting points were set according to the Central Disaster Management Council [14]. Fig.3 shows the fault models of Case 1, Case 2, and Case 3. In this figure, the slip displacement and stress drop for each asperity also are shown.

4. Element earthquakes for ground motion estimation

As element earthquakes for the empirical Green's function method in this study, we took four intraslab earthquakes used by Miyakoshi *et al.* [15] and an earthquake of April 1, 2016 that occurred off the southeastern coast of Mie Prefecture in the vicinity of the plate boundary of the Nankai Trough. Regarding the above five earthquakes, the October 31, 2000, earthquake was designated as EQ01; the February 23, 2001, earthquake as EQ02; the April 3, 2001, earthquake as EQ03; the January 6, 2004, earthquake as EQ04; and the April 1, 2016, earthquake as EQ05. The epicenters of these five earthquakes are indicated by the red stars in Fig. 3 (a). The parameters of EQ01 to EQ04 were taken from Miyakoshi *et al.* [15]. Specifically, the seismic moment M_0 of each earthquake was from F-net, the stress drops of EQ01 and EQ03 were from Sato [17], and the stress drops of EQ02 and EQ04 were set based on the observation records obtained at the Sannomaru (NGY) site in Aichi Prefecture, Japan. As for EQ05, the seismic moment M_0 was from F-net, and the stress drop was calculated by using observation records at underground points of KiK-net of which

Table 2 – Fault parameters of element earthquakes

	origin time	depth [km]	moment magnitude M_W	seismic moment*1 M_0[Nm]	slip D[m]	fault area S[km^2]	stress drop*2 $\Delta\sigma$[MPa]
EQ01	2000/10/31 1:42	38	5.4	1.70×10^{17}	0.59	4.65	41.3
EQ02	2001/2/23 7:23	32	4.9	2.43×10^{16}	0.39	0.99	60.0
EQ03	2001/4/3 23:57	35	5.2	8.17×10^{16}	0.30	4.32	22.2
EQ04	2004/1/6 14:50	40	5.2	6.74×10^{16}	0.17	6.46	10.0
EQ05	2016/4/1 11:39	14	5.8	4.90×10^{17}	1.17	10.23	36.5

We assumed μ=6.22×10^{10} N/m^2 and β=4.41 km/s for EQ01 to EQ04 and μ=4.10×10^{10} N/m^2 and β=3.82 km/s for EQ05.
*1) F-net
*2) Stress drops for EQ01 and EQ03 are taken from Satoh (2003). We estimated the stress drops for EQ02 and EQ04 by using the records at NGY (Sannomaru), and the stress drop for EQ05 by using the reccords in the soil with S-wave velocity over 2 km/s at KiK-net stations within 200 km from the source.

Table 3 – Confidence upper limit periods of ground motion records at the evaluation sites from element earthquakes

	site	code	upper limit
nearer to the epicentres	Sannomaru	NGY	6 s
	Kariya	AICP12	6 s
	Yokkaich	MIEP02	10 s*
	Hamamatsu#	SZO024	10 s*
other sites	Yokkaich KiK-net	MIEH01	6 s
	Ichinomiya	AICP05	6 s
	Tsushima	AICP10	7 s
	Nishio	AICP15	6 s
	Tokai	AICP24	10 s*
	Toyohashi	AIC015	10 s*
	Nagoya Station#	NGYSTA	10 s*

Because records were not obtained at Hamamatsu from EQ04 and at Nagoya Station from EQ01 to EQ05, we estimated pseudo empirical Green's functions based on the records in the neighbors.
* 10 s means a longer upper limit than 10 seconds.

epicenter distance was within 200 km and S-wave velocity was 2 km/s or more. Table 2 lists the fault parameters of the element earthquakes.

Table 3 shows the presence or absence of observation records of the five element earthquakes at the ground motion evaluation sites, and the confidence upper limit period in the long-period range of each record. The observation records of EQ1 at Hamamatsu (SZO024) in Shizuoka Prefecture and those of EQ3 at Yokkaichi (MIEP02) in Mie Prefecture were not used as element earthquakes, because noise was contained in them. Because the observation records were not obtained at Hamamatsu (SZO024) for EQ04, the element earthquakes were estimated from the observation records at KiK-net Hamamatsu (SZOH28) by using the pseudo-empirical Green's function method (Takahashi *et al.* [18]) with reference to the ratio of the ground amplification factor at Hamamatsu (SZO024) to that at KiK-net Hamamatsu (SZOH28). Also, since no seismic observation records were obtained at Nagoya Station (NGYSTA) in Aichi Prefecture, the element earthquake motions were estimated from the records of seismic observation stations around Nagoya Station by using the same method as EQ04 at Hamamatsu (SZO024).

The assignments of the element earthquakes were configured according to the relationship between their epicenters and focal depths and the location of each subfault of the assumed fault models. Since the focal depth of EQ05 was 14 km, EQ05 was assigned to subfaults shallower than 15 km. The element

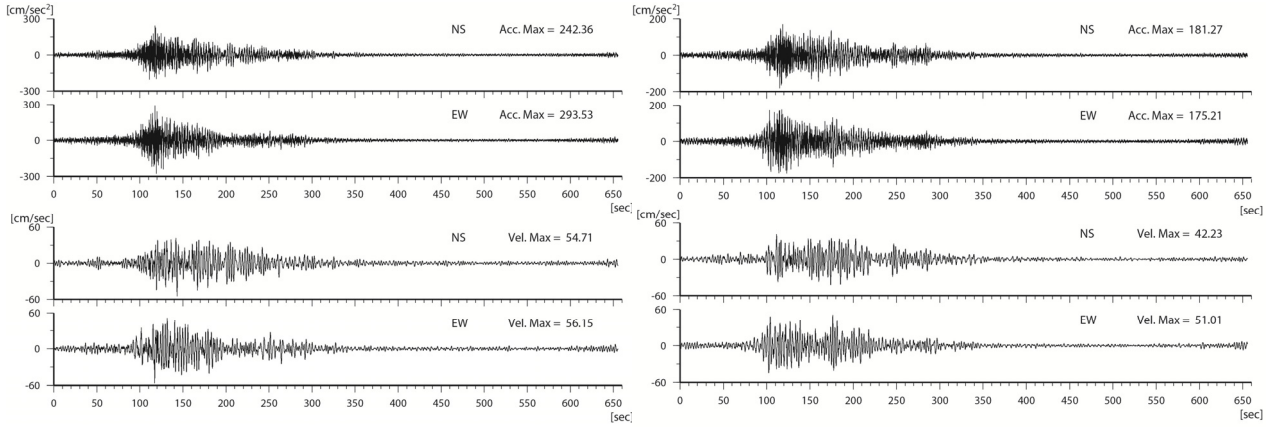

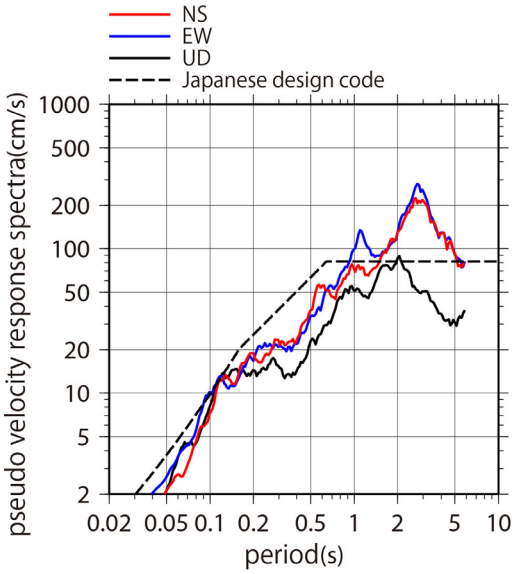

Fig. 4– Simulated waves on the ground surface of Sannomaru (NGY) site (Case 1)

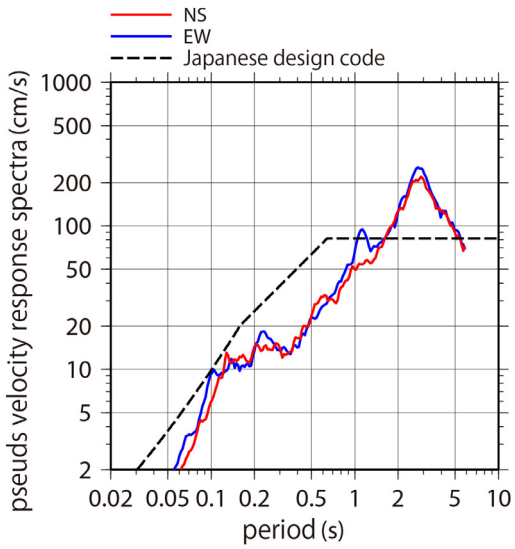

Fig. 5 – Simulated waves on the engineering bedrock of Sannomaru (NGY) site (Case 1)

earthquakes EQ01 to EQ04 were assigned so that they were closest to subfaults 15 km deep or deeper. The assignments of the element earthquakes are shown in Fig.3 (a).

5. Ground motion evaluation

5.1 Ground-motion evaluation method

Using the fault models established in Section 3 and the observation ground motion records as element earthquakes shown in Fig.3(a), ground motions were calculated on the ground surface by the empirical Green's function method. The ground motion evaluation sites were shown in Fig.1.

In the calculation of the ground motion, 11 patterns of waveforms were obtained for each component (NS, EW, and UD) because 11 patterns of seismic radiation positions were arranged randomly on each subfault. A simulated wave with the average spectral characteristic among them was created as follows. At first, pseudo velocity response spectra with a 5% damping factor were calculated for 11 patterns of the waveforms of each component. Next, the average pseudo velocity response spectrum of each component was extracted. Then, time histories were calculated to have the average response spectrum. At this time, the phase of each waveform was used. Finally, the waveform of which maximum velocity was the median value among the 11 patterns of the calculated waves was selected as a simulated wave on the ground surface. Here,

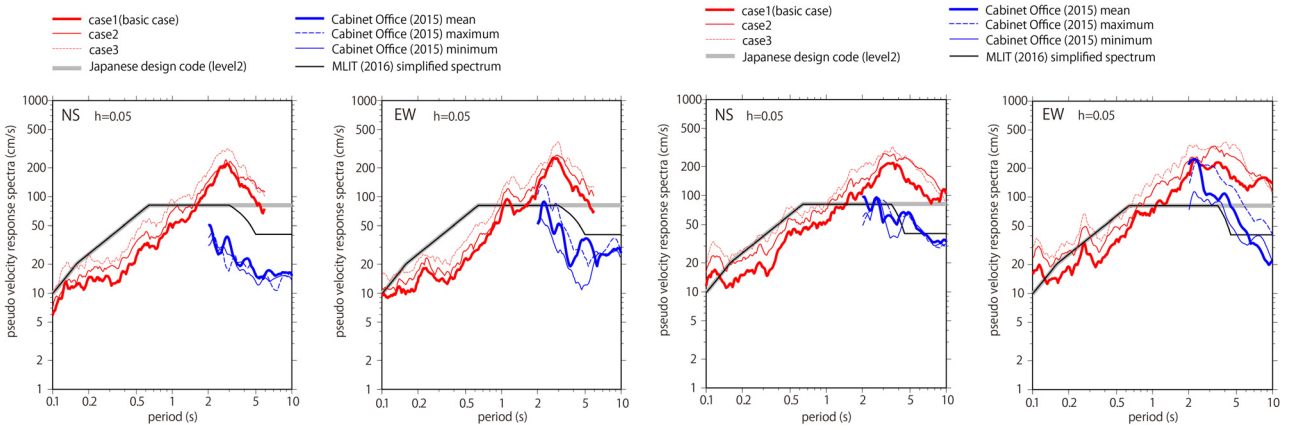

(a) Sannomaru (NGY) NS (b) Sannomaru (NGY) EW (c) Hamamatsu (SZO024) NS (d) Hamamatsu (SZO024) EW

Fig. 6 – Comparison of the results in this study with long-period ground motions by the Cabinet Office and MLIT

the maximum velocity was sorted in descending order of the two horizontal components under the condition that the random parameter was the same for three components of each pattern.

On the other hand, waves on the engineering bedrock were calculated from the 11 patterns of ground motions by the empirical Green's function method based on the one dimensional wave propagation theory. Using calculated above mentioned, 11 patterns of simulated waves were calculated on the engineering bedrock. Furthermore, a simulated wave on the engineering bedrock was selected in the same way as the simulated wave on the ground surface was selected.

5.2 Ground motion evaluation results

Fig.4 shows the waveforms and pseudo velocity response spectra (h=5%) of the simulated waves on the ground surface at the Sannomaru (NGY) site for Case 1, in which the short period level was the average value of the empirical formula by Dan *et al.* [10]. Fig.5 shows those of the simulated waves on the engineering bedrock. Fig.6 shows pseudo velocity response spectra (h=5%) of the simulated waves on the engineering bedrock at the Sannomaru (NGY) site and the Hamamatsu (SZO024) site for Case 1, Case 2, and Case 3. The design spectrum for Level2 proposed by MLIT and those for three cases calculated by the Cabinet Office [4] were shown together in these figures, which are mentioned later in 5.3.2. From Fig.4 and Fig.5, it is found that a predominant period of the simulated wave on the ground surface at the Sannomaru (NGY) site is around 3 s. This corresponds to the primary dominant period of the deep subsurface structure at this site. From Fig.6, it can be seen that the ground motion level increases in the order of Case 1, Case 2, and Case 3.

5.3 Discussion of ground motion evaluation results

5.3.1 Comparison with seismic intensity of past earthquakes

The JMA instrumental seismic intensities of the simulated waves on the ground surface were compared with the seismic intensities of past earthquakes (the 1707 Hoei earthquake, the 1854 Ansei-Tokai earthquake, and the 1944 Tonankai earthquake) estimated from the damage (Iida [19]). Fig.7 shows a comparison of the JMA instrumental seismic intensities of the simulated waves and the seismic intensities of past earthquakes at four sites (NGY Sannomaru, AICP12 Kariya, SZO024 Hamamatsu, and MIEP02 Yokkaichi). The seismic intensity of past earthquakes were converted into the JMA instrumental seismic intensities and expressed as a value with a range. From the figure, the JMA instrumental seismic intensities of the simulated waves on the ground surface for the three cases, which were evaluated considering the uncertainty of the short-period level, were within the range of the seismic intensities of past earthquakes.

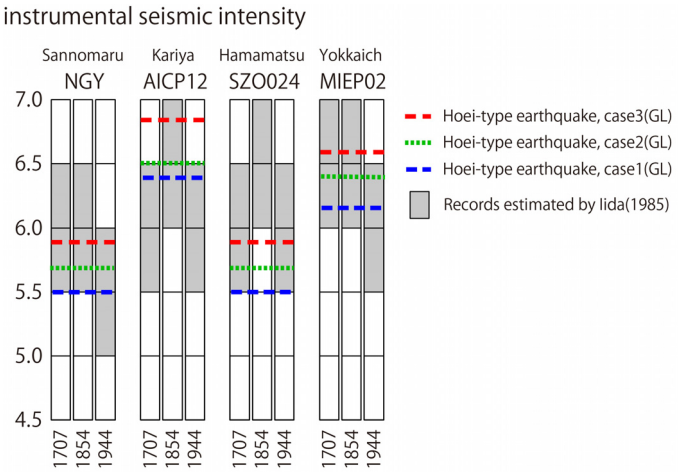

Fig. 7 – Comparison of the results in this study with seismic intensities of past earthquakes

5.3.2 Comparison with ground-motion evaluation results by other organizations

The simulated waves on the engineering bedrock were compared with the calculation results of the long-period ground motions calculated by the Cabinet Office [4] and MLIT [5].

The Cabinet Office [4] assumed a fault model consisting only of strong motion generation areas for the Hoei earthquake and evaluated long-period ground motions with periods of 2 s or longer by the three-dimensional finite difference method. Because the variety of the rupture velocity was taken into consideration for the seismic ground motion evaluation, three cases, in which the average pseudo velocity response spectra with a 5% damping in the period of 2 to 6 s were maximum, minimum, and intermediate, were shown here. Note that the ground motion of a 250m mesh including the calculation site was selected as the evaluation results of the Cabinet Office [4] for comparison. MLIT [5] conducted ground motion evaluations for the Hoei earthquake and established the design response spectra of ground motions in Kanto area, Shizuoka area, Chubu area, and Osaka areas, after formulating an empirical method using observation records including long-period ground motions.

Fig.6 shows the pseudo velocity response spectra with a 5% damping factor comparing the simulated waves on the engineering bedrock at the Sannomaru (NGY) and Hamamatsu (SZO024) sites with the ground motions by the Cabinet Office [4] and MLIT [5]. From these figures, at the Sannomaru (NGY) site, it was found that differences were observed in the vicinity of periods of 2 to 5 s of the response spectra and that the simulated waves on the engineering in this paper were the largest and the ground motion by the Cabinet Office was the smallest. At the Hamamatsu (SZO024) site, the simulated waves on the engineering bedrock in this study were slightly larger than the others, and the ground motions both of MLIT and the Cabinet Office generally corresponded to each other. The main causes of these differences can be considered as follows. MLIT used the observation records at the Hamamatsu (SZO024) site but did not use those at the Sannomaru (NGY) site, and modeling of the soil amplification characteristic was not always the same as our study. In addition, MLIT averaged the response spectra at multiple sites in the segmented area for each period band. On the other hand, the calculation results were not averaged in this study as MLIT did.

6. Response analyses of long-period buildings

Here, representative building models of high-rise buildings and base-isolated buildings were made, and nonlinear dynamic response analyses were performed for these buildings by using the ground motions evaluated in Section 5, and then earthquake proof measurements on the buildings were discussed. As a policy of the study, the building models were compiled in the initial stage of earthquake resistant design so that designers could easily determine the building scale and structure type and so on referring to the results in

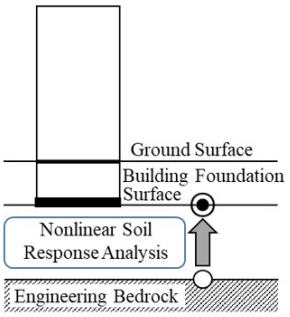

Fig.8-The estimation point of the input ground motions

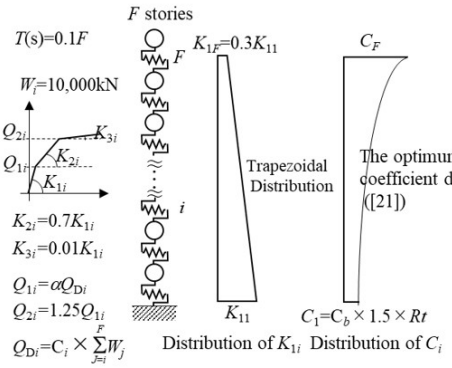

Fig.9-Analysis models of the high-rise buildings

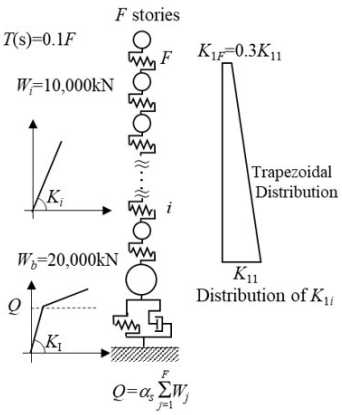

Fig.10-Analysis models of the base-isolated buildings

this study. Specifically, a goal is set as that designers can roughly grasp rational structure types that can improve safety and economy of the building through the results of parametric studies such as the number of stories, earthquake resistance strength, damping factor of the building, and the base-isolation period of the base-isolated building. The input ground motions at the foundation bed level (hereinafter the "foundation bed wave") were applied to the response analyses. These input ground motion were calculated by the earthquake response analysis considering the nonlinearity of the subsurface layer (Nishizawa *et al.* [20]). Here, the basement ground motions of Case 1 at the Sannomaru (NGY) site, which had relatively good subsurface conditions, were used as input ground motions as shown in Fig.8.

6.1 Overview of assumed building models

Figs.9 and 10 are the schematics of the analysis models treated in this study. The building models were set as follows. All floors of the building were the same type. The building weight of each floor was assumed to be 7 kN/m^2. This is equivalent to the weight per floor area of a typical steel structure high-rise building. The planar form of the building was assumed to be a square with sides of 37.8 m, so that the weight of each floor W_i was 10,000 kN. The story height of the building was 4 m. The primary natural period T (s) of the building was calculated by using the formula T (s) = 0.025 ×H (m) , which was an average relationship between T (s) and the building height H (m). Since every story height is 4 m, if the number of stories is F, then the primary natural period of the building is easily expressed as T (s) = 0.1 × F. The initial stiffness distribution of the building was a trapezoidal distribution of 0.3 at the top and 1.0 at the bottom referring to the analysis results of stiffness distribution based on the performance evaluation data about existing high-rise buildings. The ratio of the second stiffness K_{2i} to the first stiffness K_{1i} of each story was set at 0.7, and the third stiffness was $K_{3i} = 0.01 \times K_{1i}$. For the shear strength of each story, first, the design base shear coefficient C_b was set based on the relationship between design base shear coefficients and primary natural periods of buildings, and the design base shear coefficient of the building model was assumed to be C_b ×1.5× Rt, which is the structural characteristic coefficient of the building standard law in Japan. The optimum shear force coefficient [21] was used for the shear strength distribution in the height direction. Further, the ratio of the story shear force of the first breakpoint Q_{1i} to the design story shear force Q_{Di} (that is, Q_{1i} / Q_{Di}) was set in the range of 1.5 to 2.5 (referred to as the hysteresis model parameter "α"). The ratio of the shear force of the second breakpoint Q_{2i} to Q_{1i} (that is, Q_{2i} / Q_{1i}) was assumed to be 1.25. For details of the modeling, see the reference literature [20].

6.2 Results of high-rise building responses

The study was performed using several building models by changing the building height, the index α, and damping factor h. Here, we explain the results of the case of a 30-story model with α = 2 and h = 3% as an example. In this case, a primary natural period of the building is 3 s, which closely coincides with the predominant period of the deep basin in Nagoya City. In addition, α = 2 coincides with a degree of the shear

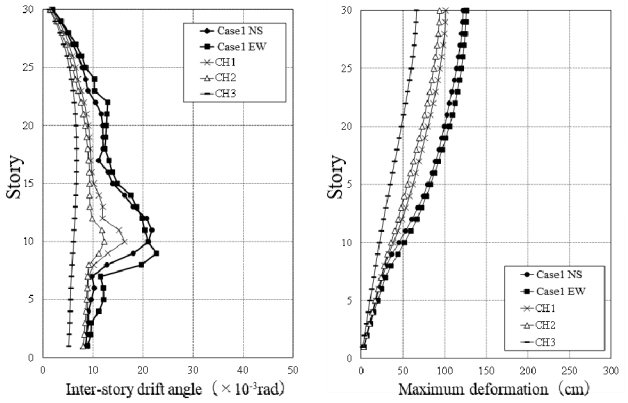

Fig. 11 – Responses of the high-rise buildings (30 stories, $\alpha = 2$, $h = 3\%$)

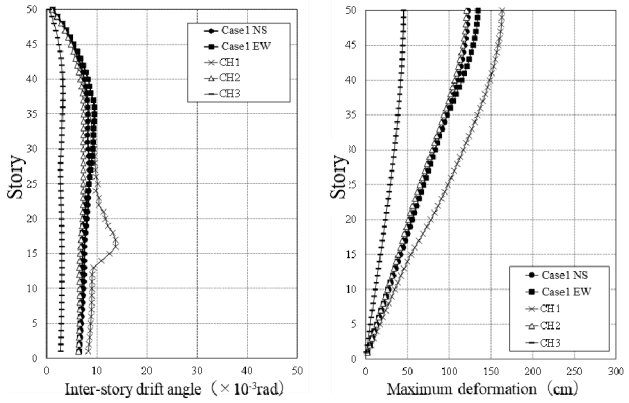

Fig. 12 – Responses of the high-rise buildings (50 stories, $\alpha = 2$, $h = 3\%$)

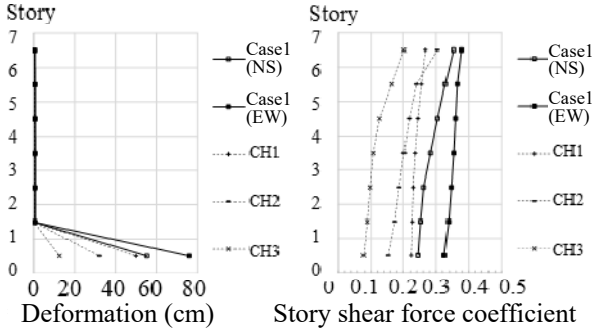

Fig. 13 – Responses of the base-isolated buildings (T=3 s, α_s= 3%)

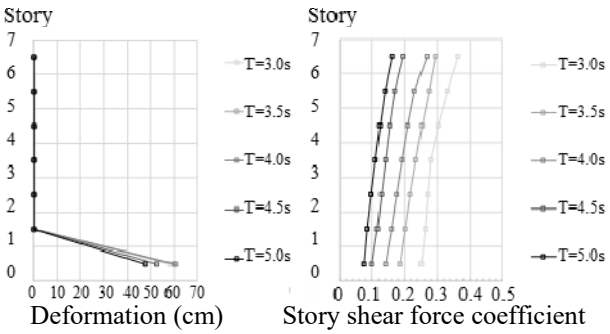

Fig. 14 – Responses of the base-isolated buildings (Case 1, T= 3 to 5 s, $\alpha_s = 4\%$)

strength of current buildings, and $h = 3\%$ corresponds to the assumption of a building with a modest addition of dampers.

Fig.11 shows the response results for the foundation bed waves of Case 1 comparing with the ground motions in CH1, CH2, and CH3 where design response spectrum level was defined for high-rise buildings or base-isolated buildings in Chubu region by MLIT [5]. Although the maximum inter-story drift angle for CH3 is less than 1/100, those of the foundation bed waves exceed 1/50. Furthermore, the responses to the foundation bed waves are larger than those to CH1 and CH2. Although the ground motions by MLIT [5] cannot be simply compared with the results for the foundation bed waves because the waves of MLIT [5] were estimated at the engineering bedrock, the foundation bed wave is larger than that of MLIT [5].

Fig.12 shows the results for a 50-story model with $\alpha = 2$ and $h = 3\%$ as another example. The primary natural period of the building is 5 s, which is different from the predominant period of the deep basin. In this case, the maximum inter-story drift angle due to the foundation bed wave is less than 1/100, for which the design is considered to be achievable with general criteria. In this case, CH1 has the largest response.

6.3 Base-isolated building response results

As in the previous sub-section 6.2, the response results for the foundation bed waves of Case 1 are shown in comparison with the response results for the ground motions of MLIT [5]. As an example of a base-isolated building without special measurements, Fig.13 shows the analysis results of a base-isolated building model with a base isolation period of 3 s, which is assumed from the strain of the isolator under the input motion of

Level2, and a damper yield shear force coefficient α_s = 3%. From this figure, it is found that the shear force coefficient acting on the building is large, so the base-isolated building having these parameters is not suitable in Sannomaru (NGY) site.

Fig.14 shows the results (Case 1) of a study in which the amount of damper was increased to α_s = 4% as a measurement against the long-period ground motion, and the base isolation period was changed. It can be seen that by setting the base isolation period to 4 s or longer, both the story shear force coefficient and the deformation of the base isolation of the building reach to the possible levels for designing with general seismic isolation criteria. Conversely, when the base isolation period is 3 or 3.5 s, which is close to the predominant period of the deep basin, the story shear force coefficient of the building increases, and it is necessary to make the period of the base isolator longer.

7. Conclusions

This paper described the results of the study for the Council aiming at evaluating design input ground motions in the Tokai region, Japan for the Nankai Trough mega-quake. We selected 11 ground motion evaluation sites and set fault models assuming the Hoei-type earthquake. We calculated ground motions by the empirical Green's function method using five element earthquakes. At that time, three cases were considered as fault models due to the uncertainty of the short-period level.

Next, the calculated ground motions were compared with the seismic intensities of past earthquakes along the Nankai Trough and the results of ground motion evaluations by other organizations. Finally, seismic response analyses were performed by considering the nonlinearity of the subsurface layer using the engineering-bedrock ground motions of Case 1 calculated at the Sannomaru (NGY) site in Aichi Prefecture, Japan. In addition, seismic response analyses of virtual building models were performed by using the ground motion at the foundation bed level as the input ground motions. Some assumed high-rise buildings and seismic-isolated buildings were used for these analyses. We showed the results of parametric study as to the number of stories, earthquake resistance strength, damping factor of the buildings, and the seismic isolation period in the case of a seismic-isolated building. It was demonstrated that amplitudes of some estimated input ground motions were large but, on the other hand, these were levels that we can conduct the seismic design by appropriate measures for both high-rise buildings and base isolated buildings.

Acknowledgments

This research was conducted as part of the Aichi Prefecture Design Input Ground Motion Creation Project and was based on the opinions of the Aichi Prefecture Design Input Earthquake Ground Motion Research Council and Working Group. We would like to express our appreciation to everyone involved in the project. We are grateful to local governments in Tokai region for their providing us with the observation records and to the National Research Institute for Earth Science and Disaster Resilience for their providing us with the records of the K-NET and KiK-net and the CMT solutions of F-net.

References

[1] N. Fukuwa, T. Kubo, K. Iyoshi, M. Onishi, T. Sato: Development of design ground motion for Nagoya, Aichi Prefecture, part 1: Overall plan outline [in Japanese], Summaries of Technical Papers of Annual Meeting Architectural Institute of Japan, pp. 81–82, 2001.9.

[2] Cabinet Office: Seismic intensity distribution and tsunami height according to a Nankai Trough megaquake (first report) [in Japanese], http://www.bousai.go.jp/jishin/nankai/model/pdf/1st_report.pdf, 2012.3.

[3] Cabinet Office: Committee for Modeling a Nankai Trough Megaquake (Second Report) (published August 29, 2012), Strong earthquake fault models: Strong earthquake fault models and seismic intensity distributions [in Japanese], http://www.bousai.go.jp/jishin/nankai/nankai/pdf/20120819_2nd_report05.pdf , 2012.8.

[4] Cabinet Office: Report on long-period ground motion due to a megaquake along the Nankai Trough [in Japanese], 2015.12.

[5] Ministry of Land, Infrastructure, Transport and Tourism: Measures for skyscrapers etc. against long-period ground motion due to a megaquake along the Nankai Trough, [in Japanese] http://www.mlit.go.jp/report/press /house05_hh_ 000620.html, 2016. (see 2017.7.18).

[6] J. Tobita, N. Fukuwa, M. Nakano, K. Yamaoka: Development of on-line data acquisition system for strong motion seismic records and its application to existent observation systems [in Japanese], Journal of Architecture and Building Science, No. 13, pp. 49–52, 2001.7.

[7] Cabinet Office: Committee for Modeling a Nankai Trough Megaquake, 15th meeting, 2012.

[8] K. Dan, Y. Ishii, J. Miyakoshi, H. Takahashi, M. Mori, N. Fukuwa: Modeling of fault rupturing of subduction plate-boundary earthquakes with magnitude 9 for predicting strong motions: Application to the Nankai trough and examples of strong motions predicted in Tokai region [in Japanese], Journal of Structural and Construction Engineering, No. 692, pp. 1685–1694, 2013.10.

[9] Headquarters for Earthquake Research Promotion/Earthquake Investigation Committee: Strong motion prediction method ("Recipe") for earthquakes with an epicenter identified to be on a fault [in Japanese], 2017.4.

[10] K. Dan, M. Watanabe, T. Sato, T. Ishii: Short−period source spectra inferred from variable−slip rupture models and modeling of earthquake faults for strong motion prediction by semi−empirical method [in Japanese], Journal of Structural and Construction Engineering, No. 545, pp. 51–62, 2001.7.

[11] T. Satoh: Source modeling of the 2011 off the Pacific coast of Tohoku earthquake using empirical Green's function method: From the viewpoint of the short period spectral level of interplate earthquake [in Japanese], Journal of Structural and Construction Engineering, No. 675, pp. 695–704, 2012.5.

[12] H. Kawabe, K. Kamae: Modeling of the of the source of the 2011 Great East Japan earthquake [in Japanese], Proceedings of the Japan Association for Earthquake Engineering, Vol. 13, No. 2, pp. 75–87, 2013.

[13] S. Kurahashi. and K. Irikura: Short-period source model of the 2011 Mw9.0 off the Pacific coast of Tohoku earthquake, Bulletin of the Seismological Society of America, Vol. 103, No. 2B, pp. 1373–1393, 2013.5.

[14] Central Disaster Prevention Council: Reports and charts regarding Tonankai and Nankai earthquakes [in Japanese], 9th, article 2-2, 2003.12.

[15] J. Miyakoshi, T. Nakata, N. Fukuwa, A. Shibata, Y. Shirase, K. Saito: Evaluation of a foundation ground motion for earthquake-resistant improvements in Sannomaru district, Nagoya City [in Japanese], Japan Association for Earthquake Engineering, Summary of the 2004 Convention, pp. 394–395, 2005.1.

[16] Aichi Prefecture Design Input Earthquake Ground Motion Research Council: Evaluation of Aichi Prefecture design input ground motion and predictions of strong ground motion according to scenario earthquake (Revised) [in Japanese], 2005.

[17] T. Satoh: Study on the dependence and of stress drop of small and medium earthquakes on the fault type and hypocenter depth and their regional characteristics [in Japanese], JSCE Journal of Earthquake Engineering, p_048.pdf-60, 2003.

[18] H. Takahashi, N. Fukuwa, K. Hayashi, J. Tobita: Estimation of ground motion at an arbitrary point using a transfer function between two points based on a ground model and seismic observation records [in Japanese], Journal of Structural and Construction Engineering, No. 609, pp. 81–88, 2006.11.

[19] K. Iida: A selection of Professor Kumiji Iida's essays, Committee for the selection and publication of Professor Kumiji Iida's essays [in Japanese], 1985.

[20] T. Nishizawa, K. Dan, M. Mori, J. Miyakoshi, H. Takahashi, K. Umemura: How to incorporate case studies on responses to a Nankai Trough earthquake and predicted large-amplitude ground motions into seismic design [in Japanese], 2015 Annual Meeting of the Architectural Institute of Japan (Kanto), PD materials, 2015.9.

[21] H. Akiyama: Seismic Limit Design for Buildings [in Japanese], University of Tokyo Press, pp. 67–70, 1980.

